ACS APPLIED MATERIALS & INTERFACES

RESEARCH ARTICLE

www.acsami.org

Li^+- and Eu^{3+}-Doped Poly(ε-caprolactone)/Siloxane Biohybrid Electrolytes for Electrochromic Devices

M. Fernandes,[†] S. S. Nobre,[‡,§] L. C. Rodrigues,[⊥] A. Gonçalves,[#] R. Rego,[†] M. C. Oliveira,[†] R. A. S. Ferreira,[‡] E. Fortunato,[#] M. M. Silva,[⊥] L. D. Carlos,[‡] and V. de Zea Bermudez*[,†]

[†]Department of Chemistry and CQ-VR, University of Trás-os-Montes e Alto Douro, 5001-801 Vila Real, Portugal

[‡]Department of Physics and CICECO, University of Aveiro, 3810-193 Aveiro, Portugal

[⊥]Department of Chemistry, University of Minho, Gualtar, 4710-057 Braga, Portugal

[#]CENIMAT/I3N, Departamento de Ciência dos Materiais, Faculdade de Ciências e Tecnologia, FCT, Universidade Nova de Lisboa and CEMOP-UNINOVA, 2829-516 Caparica, Portugal

ABSTRACT: The sol−gel process has been successfully combined with the "mixed cation" effect to produce novel luminescent and ion conducting biohybrids composed of a diurethane cross-linked poly(ε-caprolactone) (PCL530)/siloxane hybrid network (PCL stands for the poly(ε-caprolactone) biopolymer and 530 is the average molecular weight in $gmol^{-1}$) doped with a wide range of concentrations of lithium and europium triflates ($LiCF_3SO_3$ and $Eu(CF_3SO_3)_3$, respectively) (molar ratio of ca. 50:50). The hybrid samples are all semicrystalline: whereas at n = 52.6 and 27.0 (n, composition, corresponds to the number of $(C(=O)(CH_2)_5O)$ repeat units of PCL(530) per mixture of Li^+ and Eu^{3+} ions) a minor proportion of crystalline PCL(530) chains is present, at n = 6.1, a new crystalline phase emerges. The latter electrolyte is thermally stable up to 220 °C and exhibits the highest conductivity over the entire range of temperatures studied (3.7×10^{-7} and 1.71×10^{-4} S cm^{-1} at 20 and 102 °C, respectively). According to infrared spectroscopic data, major modifications occur in terms of hydrogen bonding interactions at this composition. The electrochemical stability domain of the biohybrid sample with n = 27 spans more than 7 V versus Li/Li^+. This sample is a room temperature white light emitter. Its emission color can be easily tuned across the Commission Internationale d'Éclairage (CIE) chromaticity diagram upon simply changing the excitation wavelength. Preliminary tests performed with a prototype electrochromic device (ECD) comprising the sample with n = 6.1 as electrolyte and WO_3 as cathodically coloring layer are extremely encouraging. The device exhibits switching time around 50 s, an optical density change of 0.15, good open circuit memory under atmospheric conditions (ca. 1 month) and high coloration efficiency (577 cm^2 C^{-1} in the second cycle).

KEYWORDS: poly(ε-caprolactone)/siloxane biohybrid electrolytes, ionic conductivity, luminescence, chromaticity, electrochromic device

INTRODUCTION

It has been long recognized that polymer electrolytes (PEs) are potentially interesting as electrolytes for solid-state electrochemical devices.[1−3] The basic principle of the synthesis of conducting, solvent-free PE thin films, inherited from the host−guest concept of inorganic chemistry, is quite straightforward: it implies the dissolution of an ionic salt in a high molecular weight polymer provided that the latter contains cation-coordinating species.

Because of its extraordinary solvating ability toward salts poly(oxyethylene) (POE) has been the most widely employed macromolecule to produce PEs. The most extensively investigated POE-based systems have included lithium salts,[4] because of the foreseen applications in advanced primary and secondary batteries and electrochromic devices. Although less effort has been devoted to the investigation of PEs incorporating lanthanide salts,[5−17] these materials are attractive candidates for the fabrication of optical devices, such as fiber amplifiers, phosphors and solid-state lasers.

The poor processability and especially the marked tendency to crystallize have delayed the practical application of POE-based electrolytes. Although Gadjourova et al.[18] demonstrated recently that ionic conductivity in the crystalline domains of the host polymer can be significantly higher than in the corresponding amorphous regions, in practice the prevailing procedure nowadays follows Berthier et al.[19]'s view which supports that in semicrystalline PEs ionic transport is restricted to the amorphous phases. To overcome the drawbacks of the conventional POE-based PEs, several strategies have been proposed.[3] Among these, the addition of plasticizers, the modification of the polymer

Received: April 5, 2011
Accepted: July 20, 2011
Published: July 20, 2011

architecture and the modification of the anion design have been the most widely explored. A minor amount of works have employed the so-called mixed cation effect.

With the primary goal of developing a new family of environmentally friendly multifunctional biohybrid materials displaying simultaneously high ionic conductivity and high luminescence we have produced in the present work, by means of the sol−gel route,[20] ormolytes (organically modified silicate electrolytes) comprising biopolymer chains and have doped them with a mixture of lithium triflate ($LiCF_3SO_3$) and europium triflate ($Eu(CF_3SO_3)_3$) (molar ratio $LiCF_3SO_3$:$Eu(CF_3SO_3)_3 \approx 50:50$), in the light of the mixed cation effect. The integration of different hybrid components in a single device is of the utmost interest. This "lab-on-a-chip technology" is expected to have a tremendous impact on information and communication technologies, global health and biomedicine, structural engineering and environment monitoring systems in the near future. Requirements such as speed, sensitivity, specificity, ease of use, shelf life, cost, scalability, and recyclability are critical.[21]

The hybrid concept[22] has been adopted here because organic/inorganic hybrid structures (in particular the class of POE/siloxane matrices) are known to display a series of advantages: (1) Unlike classical PEs, they may accommodate high concentrations of guest ionic salts without "salting-out" consequences; (2) Typically, in these materials, the proportion of crystalline regions is null or very low; (3) Processing into thin films with high transparency is simple, easy, and cheap; (4) The xerogel samples exhibit improved mechanical, chemical and thermal stability. A significant number of Li^+-doped POE-based ormolytes have been investigated in the last decades.[23−32] The references dealing with POE/siloxane ormolytes incorporating europium salts are considerably less abundant.[33−35]

The mixed cation approach, which basically involves the use of two guest salts instead of a single one, is an attractive procedure that usually results in a significant enhancement of the ionic conductivity of PEs.[36−41] It is manifested in the following cases: (1) with salts containing cations of the same or different valence; (2) with salts composed of the same or different anionic species; (3) with variable relative amounts of the two salts. Although the origin of the increase of conductivity observed in PEs doped with a pair of ionic salts remains uncertain, changes in charge carrier type and concentration or in the microscopic viscosity have been pointed out as possible explanations. In some cases, however, the mixed cation effect does not emerge, a situation found for instance by Chowdary et al.[42] in systems composed of mixtures of poly(ethylene glycol) dimethylether and POE containing various ratios of zinc and lithium bromides.

In the present work we have decided to employ the d-PCL(530)/siloxane structure for two reasons: (1) The electrolyte behavior of the diurethane cross-linked d-PCL(530)/siloxane network (Scheme 1) doped with lithium triflate ($LiCF_3SO_3$)[43] and magnesium triflate ($Mg(CF_3SO_3)_2$)[44] is quite encouraging. (2) The incorporation of $Eu(tta)_3(H_2O)_2$ (tta- is 2-thenoyltrifluoracetonate) into the d-PCL(530)/siloxane matrix, not only resulted in a significant increase of the $^5D_0$ quantum efficiency value of the aquocomplex (from 29.0 to 44.2%) but also yielded a hybrid that displayed high photostability (under UVA exposure, the emission intensity decreased less than 10% in 11 h).[45]

The materials studied here have been identified using the notation d-PCL(530)/siloxane$_n$Li$_m$Eu$_{m'}$, where n (called composition) corresponds to the number of $(C(=O)(CH_2)_5O)$ repeat units of PCL(530) per mixture of Li^++Eu^{3+} ions and m and m' represent the individual compositions of $LiCF_3SO_3$ and $Eu(CF_3SO_3)_3$, respectively. The samples have been examined by means of differential scanning calorimetry (DSC), thermogravimetric analysis (TGA), X-ray diffraction (XRD), complex impedance spectroscopy, cyclic voltammetry (CV), photoluminescence (PL) spectroscopy and Fourier Transform infrared spectroscopy (FT-IR). In addition, a preliminary evaluation of the performance of an all solid-state ECD including as electrolyte the sample with the highest conductivity of the d-PCL(530)/siloxane$_n$Li$_m$Eu$_{m'}$ family has been carried out. The characteristics of this prototype ECD have been investigated by means of ultraviolet/visible (UV/vis) spectroscopy and chronoamperometry (CA) measurements.

Finally, we emphasize that the work of Morita et al.[40] focused on POE-grafted poly(methylmethacrylate) matrices doped with $LiCF_3SO_3$ and lanthanum triflate or ytterbium triflate, and is the only known study of a PE system including a mixture of an alkaline salt and a lanthanide salt. We also stress that to the best of our knowledge, this is the first time that the mixed cation approach is combined with the hybrid concept.

RESULTS AND DISCUSSION

Thermal Behavior. The well-known hygroscopic nature of the two guest triflate salts employed prompted us to examine the thermal behavior of the as-received compounds.

The TGA curve of $LiCF_3SO_3$ shown in Figure 1a reveals that the decomposition of this salt is a two-step process. Below 80 °C, an initial mass loss of ca. 4% is evident, followed by a stability plateau that ends with an abrupt mass drop stage with onset at about 425 °C. The latter event represents the main degradation stage. At 800 °C a residue that represents 15% of mass loss remains. The DSC curve of $LiCF_3SO_3$ (Figure 1a) displays an endothermic peak centered at 59 °C (T_{onset} at ca. 57 °C) that correlates well with the initial mass loss observed in the TGA curve. According to Lu et al.[46] this thermal event is due to the removal of free hydrogen fluoride (HF), a product that remains after the salt production process. The associated enthalpy (ΔH = 33 J g^{-1}) is much lower than the value reported by the same authors (164 J g^{-1}).[46] On the basis of the TGA data, we have been able to estimate that the number of HF moles initially present in the as-received $LiCF_3SO_3$ and thus deduce that the exact formula of the salt is $LiCF_3SO_3 \cdot 0.4HF$. Below 300 °C, another endothermic event, less intense than the former, slightly broader and centered at 135 °C (T_{onset} at ca. 126 °C) is detected in the DSC curve (Figure 1a). As it does not imply a mass variation (see TGA curve), it might be due to a solid state phase transition.[46] The fusion of $LiCF_3SO_3$ (423 °C) occurs shortly before its decomposition (425 °C).[46] The melting temperature is thus higher than the maximum temperature value considered in our DSC analysis (300 °C) and consequently our data do not enable us to detect this thermal event. The final residue may be associated with 1 mol of lithium fluoride (LiF).[46]

Close analysis of the TGA curve of $Eu(CF_3SO_3)_3.xH_2O$ (Figure 1b) reveals that the thermal decomposition of this compound occurs in several stages. Below 160 °C three mass losses of ca. 16% (T < 90 °C), 5% (90 < T < 137 °C), and 3% (137 < T < 160 °C) are visible. They correspond to the loss of seven, two, and one water molecules, respectively. At about 400 °C the TGA suffers an abrupt drop, which corresponds to a major, although not complete, thermal degradation of the salt. These results may be interpreted as a clear indication that three of

Scheme 1. Tentative Representation of the Chemical Surrounding of the Urethane-, Esther-, and Ether-Type Oxygen Atoms in the Host d-PCL(530)/Siloxane Hybrid

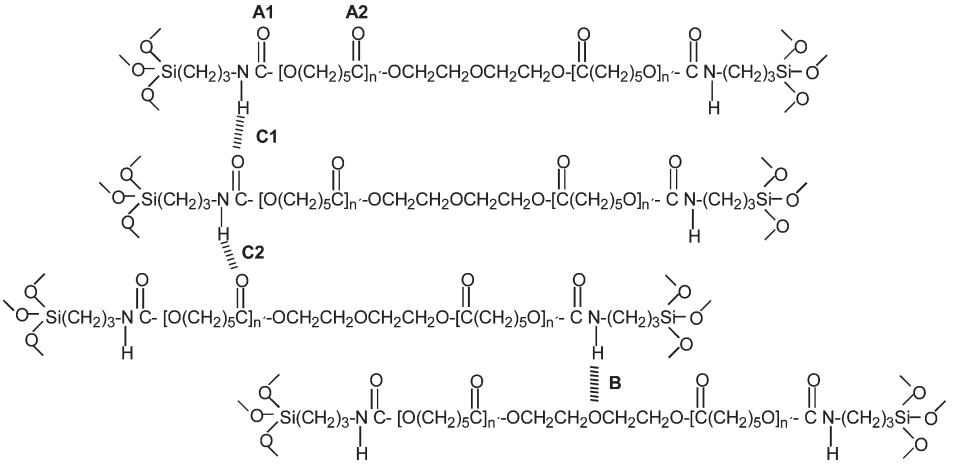

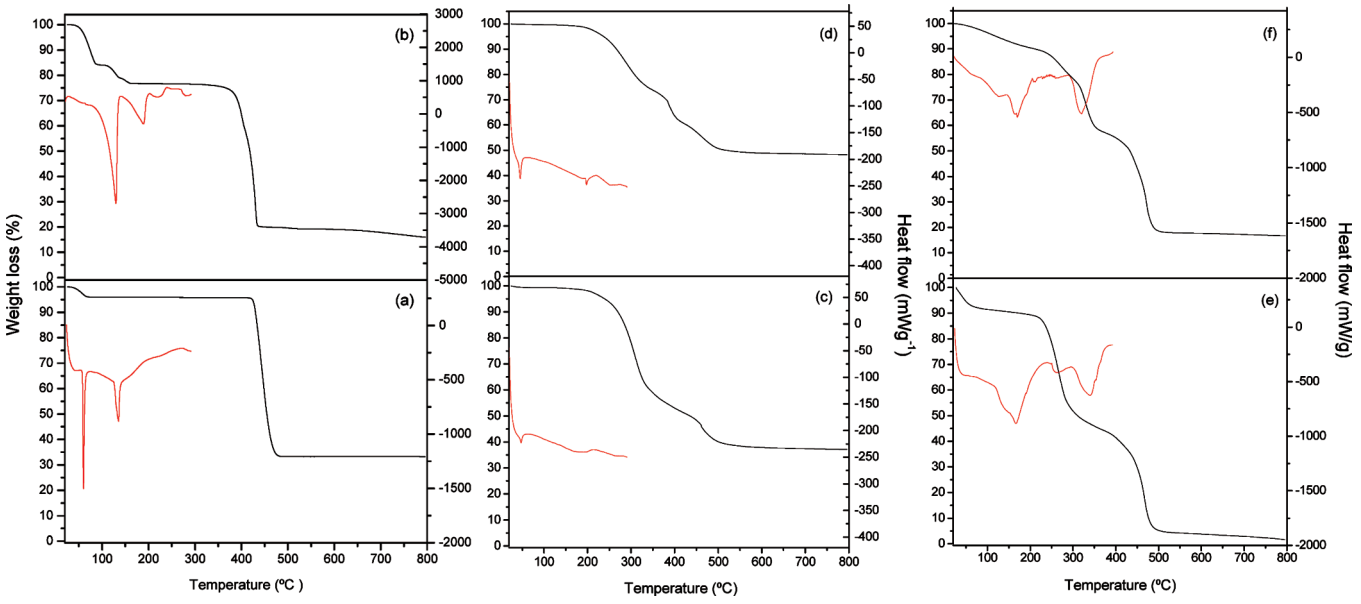

Figure 1. Thermal behavior of (a) $LiCF_3SO_3$, (b) $[Eu(CF_3SO_3)_3(H_2O)_3].7H_2O$, (c) d-PCL(530)/siloxane$_{52.6}$Li$_{99}$Eu$_{111}$, (d) d-PCL(530)/siloxane$_{27.0}$Li$_{50}$Eu$_{56}$, (e) d-PCL(530)/siloxane$_{6.1}$Li$_{12}$Eu$_{12}$, and (f) d-PCL(530)/siloxane$_{3.2}$Li$_6$Eu$_7$. The black and red lines represent the TGA (left axis) and DSC (right axis) curves, respectively.

the ten water molecules present in the decahydrated compound are strongly bonded to the Eu^{3+} ion and thus presumably belong to its first coordination sphere. Their complete removal requires temperatures of at least 160 °C. In contrast, the remaining seven water molecules are considerably more labile and may be removed readily below 90 °C through simple drying procedures. The correct formula of the compound purchased is therefore $[Eu(CF_3SO_3)_3(H_2O)_3].7H_2O$. The prominent and sharp endothermic peak centered at 129 °C (T_{onset} difficult to determine) and that less intense and broader centered at 188 °C (T_{onset} = 141 °C) discerned in the DSC curve of this salt (Figure 1b) are typical of dehydration of a compound comprising water molecules bound with different strength. The former DSC peak detected presumably corresponds to two processes: the first takes place in the low temperature range and implies the removal of the seven labile water molecules of the compound; the second process, occurring at higher temperature, represents the cleavage of the bonds that ensure strong coordination of two water molecules in the first coordination shell of the lanthanide ion. The 188 °C peak is clearly associated with the most strongly Eu^{3+}-bonded water molecule of the salt.

The TGA data reproduced in panels c and d in Figure 1 demonstrate that the thermal degradation of the d-PCL(530)/siloxane$_{52.6}$Li$_{99}$Eu$_{111}$ and d-PCL(530)/siloxane$_{27.0}$Li$_{50}$Eu$_{56}$ hybrid samples is initiated at ca. 238 and 220 °C, respectively. The TGA curves also reveal that decomposition takes place in two and three steps, respectively. Beyond about 500 °C, a plateau is attained in both cases, that persists up to the maximum temperature analyzed (800 °C). At the latter temperature the samples are not fully decomposed and a considerable amount

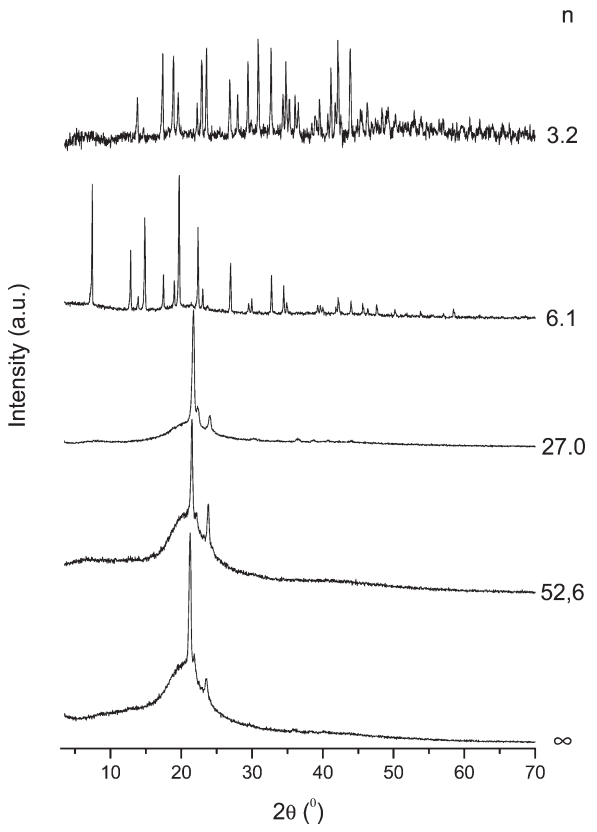

Figure 2. XRD patterns of the d-PCL(530)/siloxane$_n$Li$_m$Eu$_{m'}$ hybrids.

of residue still remains (40−45% of the sample mass). In the case of the salt-rich sample d-PCL(530)/siloxane$_{6.1}$Li$_{12}$Eu$_{12}$ (Figure 1e), after an initial mass loss of about 8%, the TGA curve is subject to two major drops at 220 °C and at about 400 °C (Figure 1e). At 800 °C the degradation of this material may be considered practically accomplished. At last, in the case of the most concentrated sample d-PCL(530)/siloxane$_{3.2}$Li$_6$Eu$_7$ (Figure 1f), thermal decomposition starts immediately from room temperature and is a multistep process below 500 °C. Between this temperature and 800 °C no mass losses occur. At the maximum temperature examined ca. 20% of the sample mass persists. It is worth noting that in the four hybrid samples examined the value of the decomposition onset temperature is lower than that reported for the nondoped d-PCL(530)/siloxane (300 °C),[43] an indication that the mixture of the two guest salts exerts a nonstabilizing effect on the host d-PCL(530)/siloxane framework. This effect is critical in the case of the most concentrated hybrid d-PCL(530)/siloxane$_{3.2}$Li$_6$Eu$_7$ (Figure 1f).

The hybrid samples with $n \geq 6.1$ are semicrystalline. In the case of the dilute d-PCL(530)/siloxane$_{52.6}$Li$_{99}$Eu$_{111}$ and d-PCL(530)/siloxane$_{27.0}$Li$_{50}$Eu$_{56}$ samples, a weak endothermic peak centered near 47 °C is seen in the DSC thermograms (Figure 1c,d), respectively). As the melting temperature of the crystalline organic precursor PCL(530) ranges from 36 to 48 °C, the thermal event found in both DSC curves is definitely associated with the fusion of a minor proportion of free, crystalline PCL(530) chains in the PCL(530)/siloxane matrix. Based on the value reported in the literature for the bulk enthalpy of melting of 100% crystalline PCL (ΔH_m^0 = 166.7 J g^{-1} [47]) and on the experimental data retrieved from the DSC thermograms of PCL(530)/siloxane$_{52.6}$Li$_{99}$Eu$_{111}$ and PCL(530)/siloxane$_{27.0}$Li$_{50}$Eu$_{56}$ samples (ΔH_m = 1.49 and 5.69 J g^{-1}, respectively), we concluded that the proportion of crystallinity in both samples is indeed negligible (0.9 and 3.4%, respectively). The formation of free crystalline PCL(530) regions in both hybrids is in perfect agreement with the presence of the pair of intense and sharp Bragg peaks characteristic of PCL(530) (not shown) at 23.8 and 21.6° in their XRD patterns (Figure 2). In both diffractograms, this pair of peaks coexists with a broad band centered near 21°, Gaussian in shape, also produced by the nondoped d-PCL(530)/siloxane structure and due to the coherent diffraction of the siliceous domains.[48] In contrast with previous results that supported the amorphous character of the nondoped matrix,[43] in the present case, the XRD pattern of d-PCL(530)/siloxane evidence the existence of crystalline PCL(530) chains (Figure 2). It is noteworthy that the formation of crystalline domains of PCL(530) was also reported in the case of d-PCL(530)/siloxane-based materials doped with the Eu(tta)$_3$(H$_2$O)$_2$ and Eu(tta)$_3$phen (phen is 1,10-phenantroline) complexes.[45] The nature of the second peak centered at 200 °C in the DSC thermogram of d-PCL(530)/siloxane$_{27.0}$Li$_{50}$Eu$_{56}$ hybrid is unknown. In the case of the d-PCL(530)/siloxane$_{6.1}$Li$_{12}$Eu$_{12}$ material, as the Bragg peaks discerned in its XRD pattern (Figure 2) do not coincide with those produced by LiCF$_3$SO$_3$ (not shown), [Eu(CF$_3$SO$_3$)$_3$(H$_2$O)$_3$].7H$_2$O (not shown) or PCL(530) (not shown), we are led to conclude that a new crystalline phase is formed. The DSC curve depicted in Figure 1f confirms that the thermal decomposition of the most concentrated sample studied is a highly complex process that is initiated immediately after the beginning of the measurement, all the endothermic peaks observed being entirely attributed to degradation reactions.

In the SEM images recorded for d-PCL(530)/siloxane$_{52.6}$Li$_{50}$Eu$_{56}$ (Figure 3c,d) and d-PCL(530)/siloxane$_{27.0}$Li$_{50}$Eu$_{56}$ (Figure 3e,f) the presence of crystalline PCL(530) chains (Figures 3a,b) is visible. As expected, the texture of these samples contrasts deeply with that reported earlier for amorphous d-PCL(530)/siloxane based materials.[50] The formation of a new crystalline phase in the d-PCL(530)/siloxane$_n$Li$_m$Eu$_{m'}$ system at high salt content is clearly recognized in the SEM images g and h in Figure 3. Images i and j in Figure 3 show the high crystalline nature of the most concentrated sample, which confirms XRD data (Figure 2).

Electrochemical Properties. High ionic conductivity (higher than 1 × 10^{-5} Scm^{-1}) is definitely one of the most important requirements that need to be fulfilled in a PE system if practical applications in electrochemical devices are envisaged. The main conclusion derived from our earlier work conducted on the d-PCL(530)/siloxane biohybrid system doped with LiCF$_3$SO$_3$ was that the conductivities exhibited by these materials are modest[43] with respect to those observed in classical LiCF$_3$SO$_3$-containing PEs extensively reported in the literature.

The Arrhenius conductivity plot of the d-PCL(530)/siloxane$_n$Li$_m$Eu$_{m'}$ biohybrids is reproduced in Figure 4a. This graph also shows the temperature dependence of the ionic conductivities of some of the PCL(530)/siloxane$_n$LiCF$_3$SO$_3$ samples studied previously.[43] Examination of Figure 4a allows us to state that the addition of a mixture of LiCF$_3$SO$_3$ and [Eu(CF$_3$SO$_3$)$_3$(H$_2$O)$_3$].7H$_2$O to the host d-PCL(530)/siloxane matrix instead of simply LiCF$_3$SO$_3$ was successful, as a remarkable enhancement of the ionic conductivity resulted,[43] a clear manifestation of the cation mixed effect. For instance, although at 25 °C the conductivity of the d-PCL(530)/siloxane$_{52.6}$Li$_{99}$Eu$_{111}$ hybrid is ca. 2 × 10^{-8} S cm^{-1}, at about 100 °C, it attains 2.3 × 10^{-6} S cm^{-1} (Figure 4a). These values are approximately 1 order of magnitude higher than those measured previously for the d-PCL(530)/

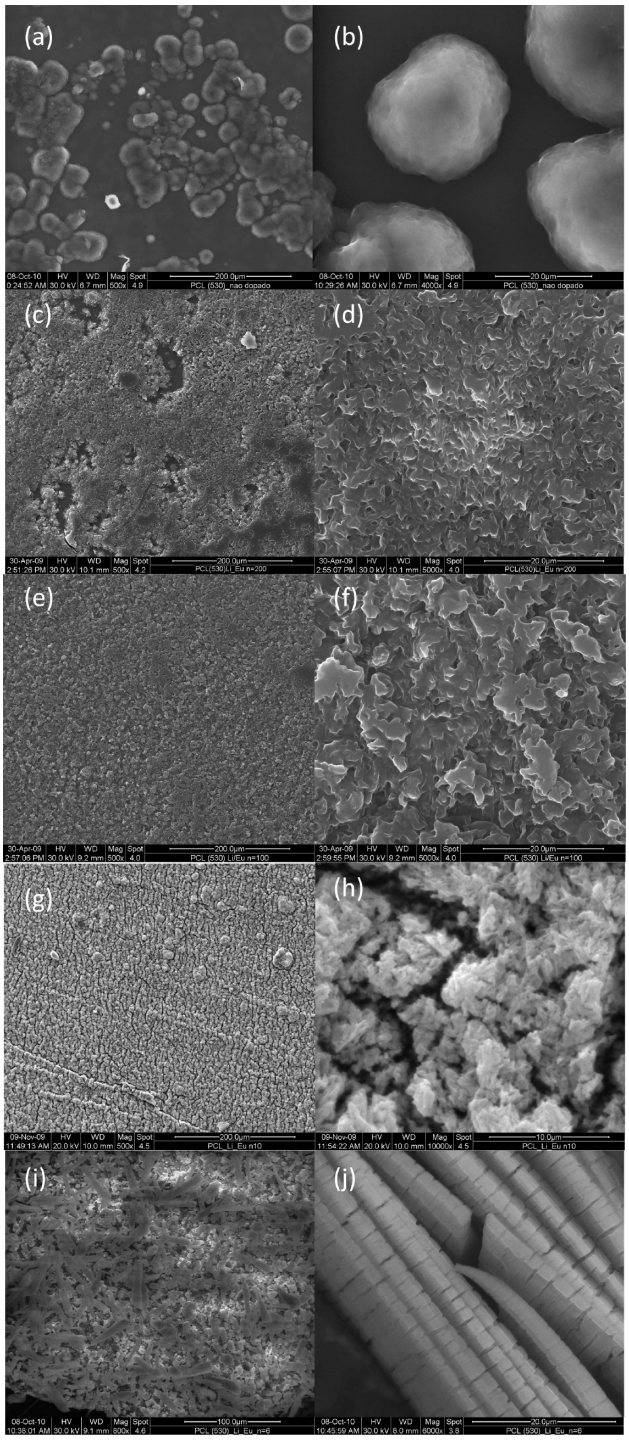

Figure 3. SEM images of the d-PCL(530)/siloxane$_n$Li$_m$Eu$_{m'}$ hybrids with $n = \infty$ (scale bars = (a) 100 and (b) 20 μm), $n = 52.6$ (scale bars = (c) 200 and (d) 20 μm), $n = 27$ (scale bars = (e) 200 and (f) 20 μm), $n = 6.1$ (scale bars = (g) 200 and (h) 10 μm) and $n = 3.2$ (scale bars = (i) 100 and (j) 20 μm).

siloxane matrix doped solely with $LiCF_3SO_3$ and $n = 93$ (5.44×10^{-9} and 5.93×10^{-7} S cm^{-1} at 27 and ~100 °C, respectively)[43] (Figure 4a). In the high temperature range (at ca. 100 °C), the conductivity of the d-PCL(530)/siloxane$_{3.2}$Li$_6$Eu$_7$ sample practically coincides with that of the most conducting composition of the d-PCL(530)siloxane$_n$LiCF$_3$SO$_3$ series ($n = 0.5$) (2.94×10^{-5} and 3.2×10^{-5} S cm^{-1}, respectively[43]). The conductivity maximum of the d-PCL(530)/siloxane$_n$Li$_m$Eu$_{m'}$ system is located at $n = 6.1$ over the whole range of temperatures studied (3.7×10^{-7} and 1.71×10^{-4} S cm^{-1} at 20 and 102 °C, respectively) (Figure 4c).

The microelectrode cyclic voltammogram of the d-PCL(530)/siloxane$_{27.0}$Li$_{50}$Eu$_{56}$ hybrid over the −2.0 to 8.0 V potential range obtained at 30 °C is depicted in Figure 5. This voltammogram demonstrates that in the anodic region the sample is stable up to about 5.0 V versus Li/Li$^+$, whereas the cathodic region lithium deposition is not detected (see Experimental Section). This means that the overall redox stability of d-PCL(530)/siloxane$_{27.0}$Li$_{50}$Eu$_{56}$ spans more than 7 V, an indication that this material displays an acceptable stability window for an application in a solid state electrochemical device. These results are in perfect agreement with those found for d-PCL(530)siloxane$_{0.5}$LiCF$_3$SO$_3$.[43]

Cation/Cross-Link, Cation/Polymer Chains, and Cation/Anion Interactions. To elucidate the role played by the carbonyl (C═O) oxygen atoms of the urethane cross-links in the coordination of the Eu^{3+} and Li$^+$ ions, we have inspected the signature of the d-PCL(530)/siloxane$_n$Li$_m$Eu$_{m'}$ hybrids in the "amide I" region of the FT-IR spectra. After incorporation into the hybrid host framework, several types of interactions may be enviasaged for the Li$^+$ and Eu^{3+} ions:[45] (1) bonding to the "free" urethane C═O groups of the cross-links; (2) bonding to "free" esther C═O groups of the PCL(530) chains; (3) bonding to C═O groups belonging to hydrogen-bonded aggregates (oxyethylene/urethane aggregates, urethane/urethane aggregates and esther/urethane aggregates).[45] Obviously, coordinating situation (3) implies the rupture of the hydrogen-bonded array formed throughout pristine d-PCL(530)/siloxane.

The "amide I" region of the diurethane cross-linked d-PCL(530)/siloxane$_n$Li$_m$Eu$_{m'}$ hybrids corresponds to the amide I region (1800−1600 cm^{-1}) of polyamides.[49] As the "amide I" modes are sensitive to the specificity and magnitude of hydrogen bonding, in general the band envelope is resolved into several individual components corresponding to different C═O environments: from "free" C═O groups (in the high-frequency range) to hydrogen-bonded associations or aggregates of variable strength (in the low-frequency range).

The "amide I" region of the FT-IR spectrum of the nondoped d-PCL(530)/siloxane matrix contains four distinct components located at about 1762, 1736, 1720, and 1692 cm^{-1}.[50] The high frequency bands at 1762 and 1736 cm^{-1} are associated with "free" C═O groups of the urethane cross-links (A1, Scheme 1)[50] and "free" C═O groups of the esther groups of amorphous PCL(530) chains (A2, Scheme 1).[51] The component at 1720 cm^{-1} is attributed to oxyethylene/urethane aggregates (B, Scheme 1), whereas the 1692 cm^{-1} feature is assigned to C═O groups belonging to considerably more ordered hydrogen-bonded urethane/urethane aggregates (C1, Scheme 1), and ester/urethane aggregates (C2, Scheme 1).[50]

Figure 6a proves that the inclusion of $LiCF_3SO_3$ and $[Eu(CF_3SO_3)_3(H_2O)_3].7H_2O$ into d-PCL(530)/siloxane produces a series of marked modifications in the environment of the C═O groups which are manifested in the "amide I" region in terms of band redistribution. Globally the incorporation of increasing amounts of the guest salts leads to a strengthening of the hydrogen bonds, to the saturation of the urethane free C═O groups A1 and to the formation of new, very strong and cation-coordinated hydrogen-bonded aggregates D. Further conclusions may be drawn from the analysis of the plot of

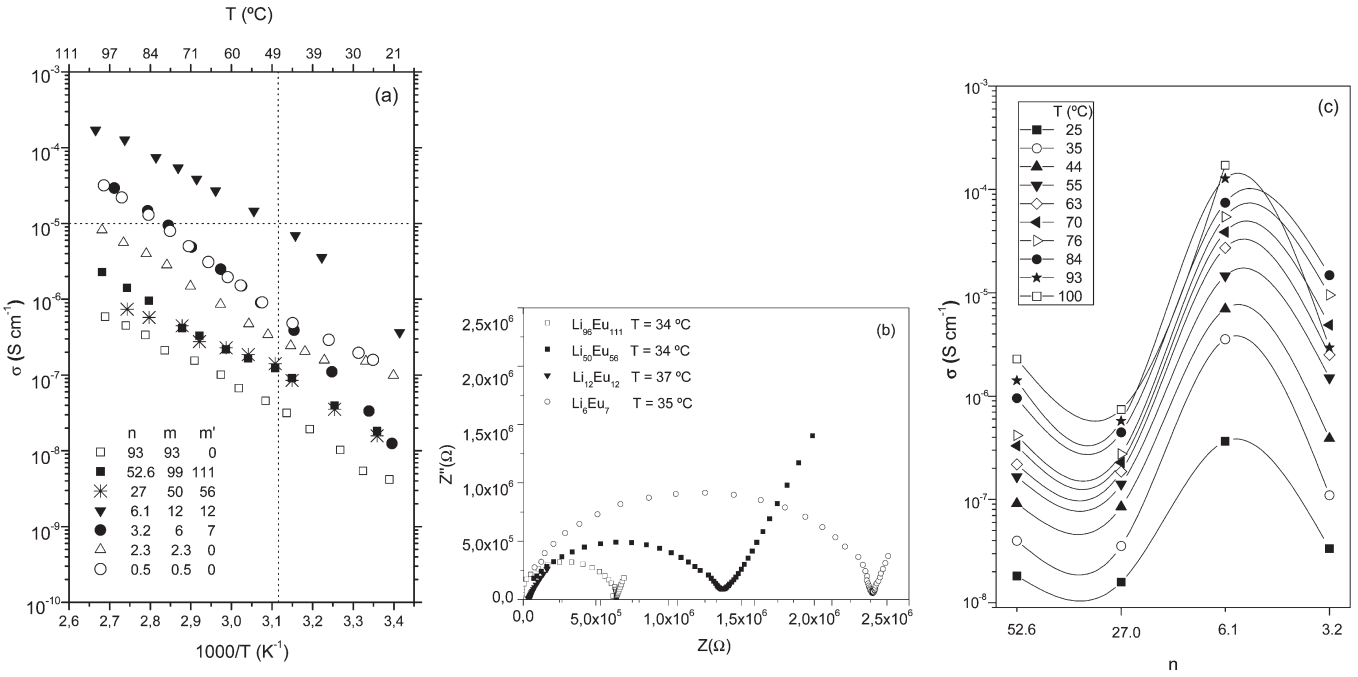

Figure 4. (a) Arrhenius conductivity plot, (b) high-frequency AC impedance Nyquist spectra and (c) isotherms of the ionic conductivity versus composition of the d-PCL(530)/siloxane$_n$Li$_m$Eu$_{m'}$ biohybrids. Note: the lines drawn are just guides for the eyes.

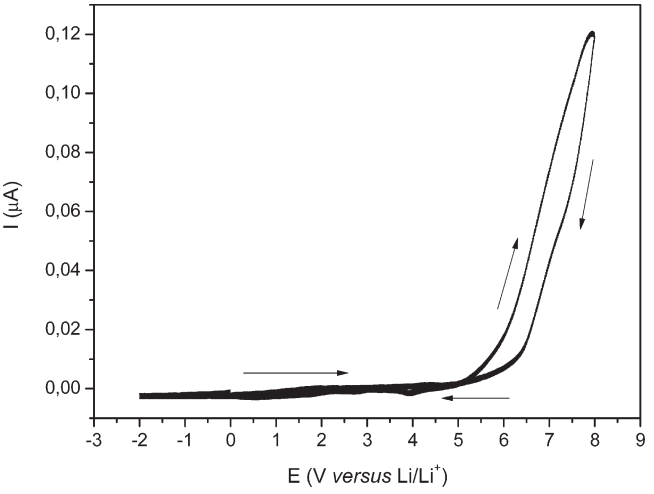

Figure 5. Cyclic voltamogram of the d-PCL(530)/siloxane$_{27.0}$Li$_{50}$Eu$_{56}$ hybrid obtained at about 30 °C with a 25 μm gold microelectrode as working electrode and lithium as counter and reference electrodes (sweep rate = 100 mVs^{-1}).

Figure 6b: (a) The fraction of "free" urethane C═O groups A1 is subject to a regular reduction. No such groups remain at n = 3.2. (b) The fraction of "free" esther C═O groups A2 increases slightly in d-PCL(530)/siloxane$_{52.6}$Li$_{99}$Eu$_{111}$ and then is significantly reduced, reaching a minimum value in the d-PCL(530)/siloxane$_{6.1}$Li$_{12}$Eu$_{12}$ material. In the most concentrated sample the proportion of these C═O groups increases, recovering the value observed at n = 27.0. (c) The most dramatic effect resulting from salts addition is undoubtedly the marked increase in the proportion of oxyethylene/urethane aggregates B which become dominant in the sample d-PCL(530)/siloxane$_{6.1}$Li$_{12}$Eu$_{12}$. At n = 3.2 a considerable fraction of these aggregates B are, however, disrupted. (d) The variation of the fraction urethane/urethane aggregates C1 with the incorporation of increasing amount of salts resembles closely that of the "free" esther C═O groups A2. This means that in samples with n = 27.0 and 6.1 a partial breakdown of these aggregates occurs, but that in contrast they are formed again at higher salt content. (e) The proportion of esther/urethane aggregates C2 does not suffer major changes over the whole salt concentration range examined, although we note a regular increase in samples with $n \leq 52.6$. (f) New hydrogen-bonded aggregates D, stronger than all the others already existent, are formed in d-PCL(530)/siloxane$_{6.1}$Li$_{12}$Eu$_{12}$. Their fraction increases in the most concentrated sample studied.

The variations detected in the integral fraction of the various C═O environments present in the d-PCL(530)/siloxane$_n$Li$_m$Eu$_{m'}$ hybrids upon introduction of increasing amounts of the two guest salts clearly point out that at n = 6.1 — the conductivity maximum of this electrolyte system — major modifications take place. This sample is very rich in oxyethylene/urethane aggregates B, formed at the expense of the breakdown of urethane/urethane aggregates C1 and of "free" urethane C═O groups A1. In parallel, a drastic reduction of the "free" esther C═O groups A2 is necessary for the formation of more esther/urethane aggregates C2 and especially of the new very strong aggregates D.

To investigate the chemical surroundings of the triflate ions at increasing content of the mixed salts, we analyzed the FT-IR spectra of the d-PCL(530)/siloxane$_n$Li$_m$Eu$_{m'}$ hybrids in the region of the symmetric stretching vibration mode of the SO_3 ($\nu_s SO_3$) group. This nondegenerated mode of the triflate ion is very sensitive to coordination effects. We note that in the light of this spectroscopic analysis the two populations of triflate ions present (i.e., that originating from $LiCF_3SO_3$ and that originating from $Eu(CF_3SO_3)_3$) are indistinguishable.

Figure 7a reproduces the $\nu_s SO_3$ region of three representative d-PCL(530)/siloxane$_n$Li$_m$Eu$_{m'}$ hybrids. The $\nu_s SO_3$ band was

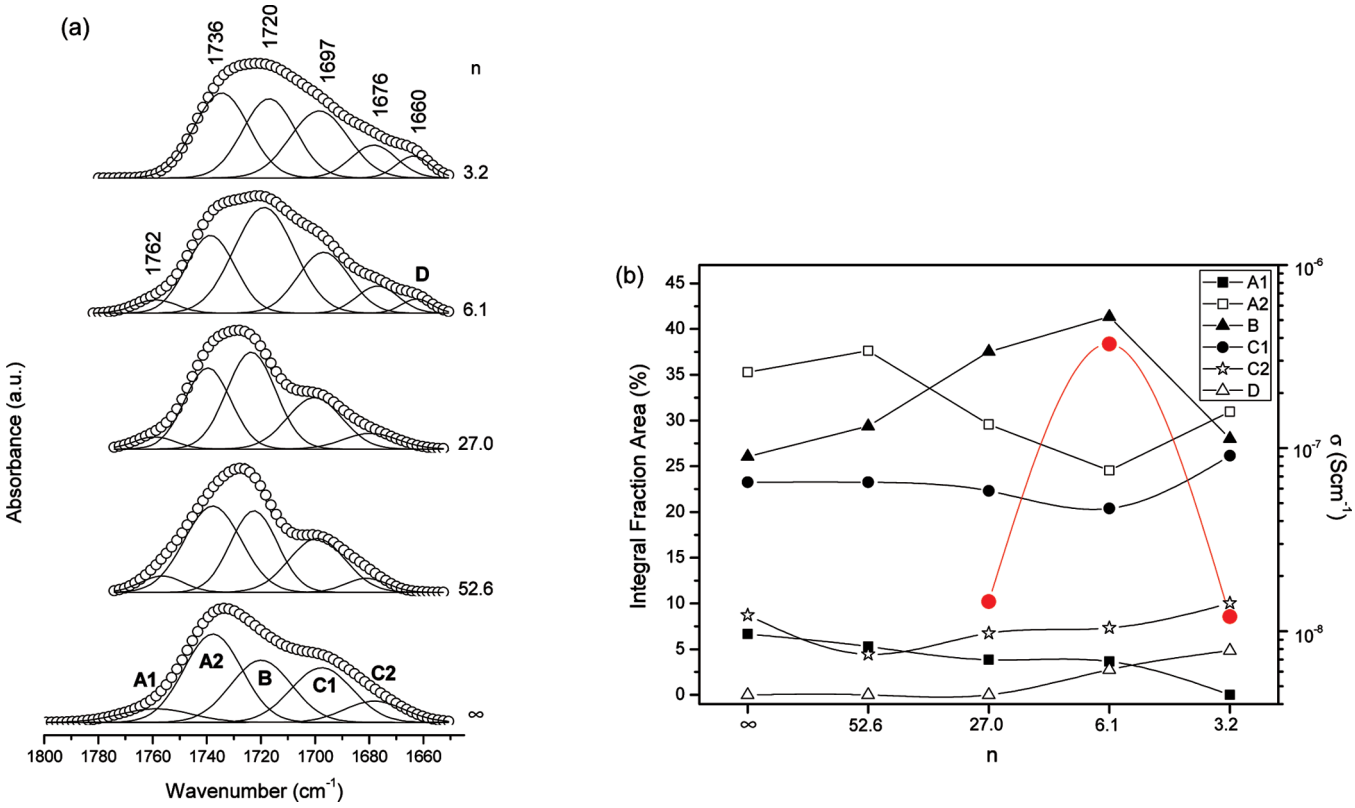

Figure 6. (a) Curve-fitting results of the "amide I" region of d-PCL(530)/siloxane$_n$Li$_m$Eu$_{m'}$ biohybrids and (b) composition dependence of the integral fraction area of the different resolved components (left axis, black curves) and of the ionic conductivity (right axis, red curve).

resolved into four components (Figure 7b): a prominent band at 1032 cm^{-1}, two shoulders positioned around 1038 and 1025 cm^{-1} and a weak peak centered at about 1045 cm^{-1}. The detection of the 1031 cm^{-1} band indicates the presence of free anions in the three samples.[52] The contribution of the so-called "cross-link separated ion pairs" to this feature is very likely.[53] The shoulders at 1038 and 1025 cm^{-1} are ascribed to weakly coordinated triflate ions located in two different anionic environments.[53] Based on the literature, the event at 1045 cm^{-1} may be associated with the formation of monodentate $Li^+CF_3SO_3^-$ ions pairs or negatively charged triplets $[Li(CF_3SO_3)_2]^-$.[54−56]

Although in the case of monourethanesil POE/siloxane compounds doped with $Eu(CF_3SO_3)_3$, we assigned the 1045 cm^{-1} band to the formation of a POE/$Eu(CF_3SO_3)_3$ crystalline compound of unknown stoichiometry,[53] in the present series of hybrids the contribution of the Eu^{3+} ions to the 1045 cm^{-1} feature is uncertain. Figure 7c shows that d-PCL(530)/siloxane$_{27.0}$Li$_{50}$Eu$_{56}$ contains a high concentration of "free" ions (1031 cm^{-1}) and weakly coordinated triflate ions (1037 cm^{-1}). Upon introduction of more salt (n =6.1) the fraction of "free" ions decreases at the expense of a further increase of the percentage of weakly coordinated anions (1037 and 1025 cm^{-1}). In addition, the proportion of associated ions is also subject to an increase (1045 cm^{-1}). In contrast with the expected situation, these trends are accompanied by a significant increase of the room temperature ionic conductivity. In the salt-rich d-PCL(530)/siloxane$_{3.2}$Li$_6$Eu$_7$ material, in spite of the fact that the fraction of "free" ions displays a slight increase and that the fraction of associated species decreases significantly, the ionic conductivity suffers a dramatic decrease.

Photoluminescence Features. Figure 8a shows the d-PCL(530)/siloxane$_{27}$Li$_{50}$Eu$_{56}$ emission under different excitation wavelengths. The emission spectra are composed of a broad band, whose energy depends on the excitation wavelength, superimposed on a series of sharp peaks attributed to the Eu^{3+} $^5D_0 \rightarrow {}^7F_{0-4}$ transitions. A similar broad emission was already observed in the nondoped d-PCL(530)/siloxane hybrid, being ascribed to electron−hole recombination occurring within oxygen-related defects present in the siliceous domains and within the cross-linkages groups.[45] The emission energy dependence on the excitation wavelength was modeled as radiative recombinations involving thermal relaxation within localized states, in the framework of the extended multiple trapping approach.[57,58] The presence of the host-related band indicates a nonefficient energy transfer d-PCL(530)/siloxane-to- Eu^{3+} ions, which in fact can be used to produce multiwavelength light-emitters. In particular, taking advantage of the relative intensity variation of the d-PCL(530)/siloxane broad band emission and of the Eu^{3+} lines, the fine-tuning of the emission color coordinates within the Commission Internationale d'Éclairage (CIE) chromaticity diagram becomes easy (Figure 8b). The emission color of the d-PCL(530)/siloxane$_{27}$Li$_{50}$Eu$_{56}$ sample can be easily tuned from the pink region (0.43,0.29) excited at 260 nm to the yellow-green area (0.37,0.54) under 464 nm, crossing the white region (0.29,0.28) at 393 nm excitation wavelength, as illustrated in the CIE chromaticity diagram.

Focusing our analysis on the intra-f^6 lines, we observe that the energy, full width at half-maximum (fwhm) and number of Stark components of the $^5D_0 \rightarrow {}^7F_{1-4}$ transitions are almost independent of the selected excitation wavelength, suggesting that the

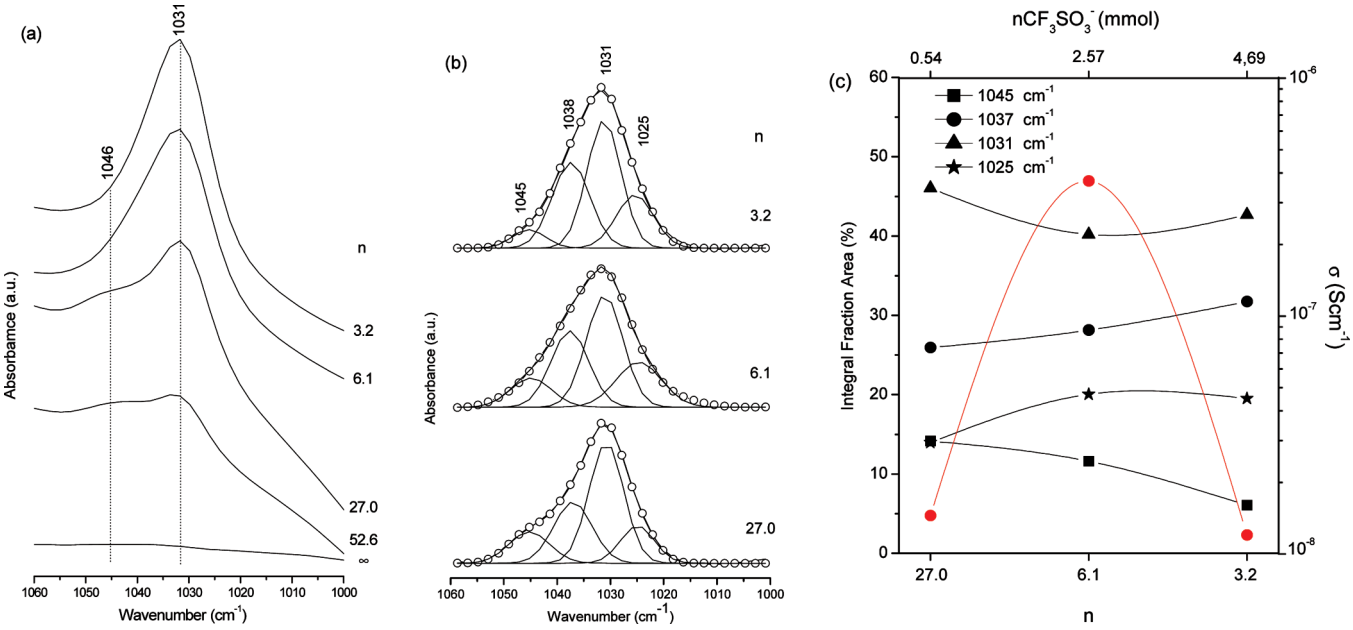

Figure 7. (a) Room-temperature FT-IR spectra of the d-PCL(530)/siloxane$_n$Li$_m$Eu$_{m'}$ hybrids in the $\nu_s SO_3$ region, (b) curve-fitting results of selected samples, (c) composition dependence of the integral area fraction of the isolated components (left axis, black curves) and the ionic conductivity (right axis, red curve).

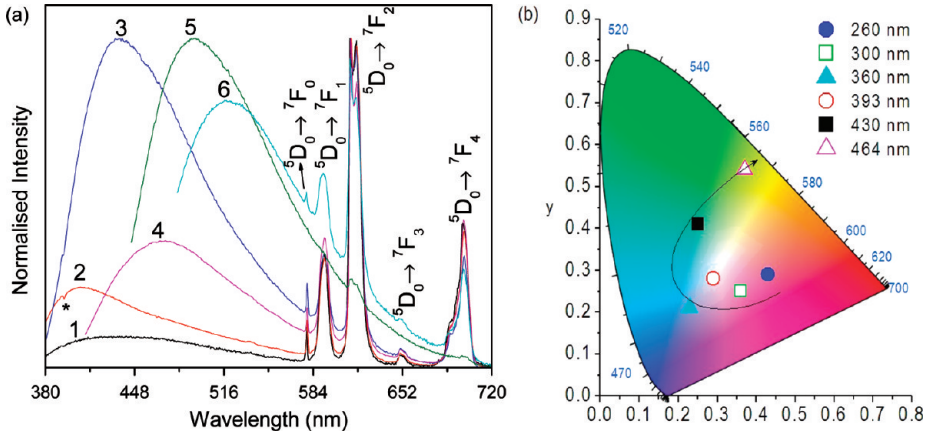

Figure 8. (a) Room-temperature emission spectra of d-PCL(530)/siloxane$_{27.0}$Li$_{50}$Eu$_{56}$ excited at (1) 260, (2) 300, (3) 360, (4) 393, (5) 430, and (6) 464 nm. (b) CIE chromaticity diagram (1931) showing the (x,y) color coordinates of the room-temperature emission excited between 260 and 464 nm.

Eu^{3+} occupy a single average local environment. Moreover, the presence of the $^5D_0 \rightarrow {}^7F_0$ line and the Stark splitting of the $^7F_{1,2}$ levels in 3 and 4 components, respectively, points out a low local-symmetry for the Eu^{3+}-coordination site with the absence of an inversion center, in agreement with the high relative intensity of the $^5D_0 \rightarrow {}^7F_2$ transition.

The emission features were further quantified by the measurement of the $^5D_0$ decay curves (monitored within the $^5D_0 \rightarrow {}^7F_2$ transition). The curves are well-reproduced by a single exponential function, in good agreement with the presence of a single average Eu^{3+}-local environment. The single exponential fit yielded $^5D_0$ lifetime values of 0.225 ± 0.001 ms and 0.262 ± 0.002 ms, for d-PCL(530)/siloxane$_{27.0}$Li$_{50}$Eu$_{56}$ and d-PCL(530)/siloxane$_{52.6}$Li$_{99}$Eu$_{111}$, respectively.

Features of a Prototype ECD. A preliminary assessment of the potential interest of the d-PCL(530)/siloxane-based ormolytes introduced here as electrolytes in an all solid-state ECDs was performed using the four layer-sandwich configuration represented in Scheme 2. We draw the attention to the fact that it did not include, as usual, an ion storage layer.[59] The outermost layers incorporated transparent conducting oxide (TCO) films made of indium-doped zinc oxide (IZO)[60] provided the electronic contacts through which a voltage difference was applied to the active layers of the device. The active layers were an electrochromic (EC) film of tungsten oxide (WO_3) and an ion conducting (IC) film of d-PCL(530)/siloxane$_{6.1}$Li$_{12}$Eu$_{12}$, the most conducting ormolyte sample of the series studied in the present work (Figure 4c).

The electrochromic contrast of an ECD may be expressed in terms of the percent transmittance change ($\Delta\%T$) at a specified wavelength (or over a specified wavelength range) for which the EC material exhibits the highest optical contrast. Optical switching

Scheme 2. Configuration of the Glass/IZO/WO_3/d-PCL-(530)/Siloxane$_{6.1}$Li$_{12}$Eu$_{12}$/IZO/Glass ECDs Investigated (polarity for the coloration mode)

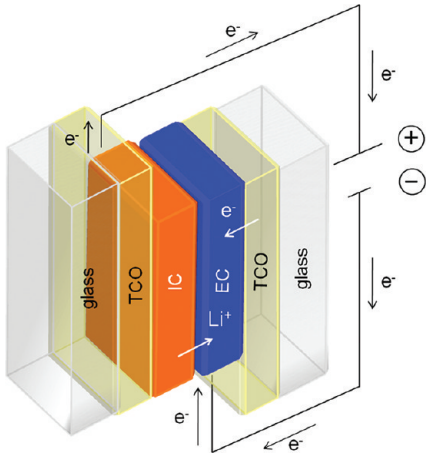

of the glass/IZO/WO_3/d-PCL(530)/siloxane$_{6.1}$Li$_{12}$Eu$_{12}$/IZO/glass ECD from light yellow to uniform dark deep blue occurred by charging/discharging the electrochemical cell through the application of a potential of −4 V and +4 V during 50 s, respectively (see pictures at the bottom of Figure 9). We note that potential values lower than this did not lead to any color change. The transmission spectra obtained in the wavelength range between 340 and 800 nm for the as-deposited, colored and bleached states are reproduced in Figure 9. All the spectra display a series of maxima and minima in this spectral region assigned to interference, resulting from the presence of a multilayer structure (Scheme 2). The average transmittance of the d-PCL(530)/siloxane$_{6.1}$Li$_{12}$Eu$_{12}$-based ECD in the VIS region (400−700 nm) is practically identical for the as-deposited and bleached states (64.6 and 60.2%, respectively), being 44.9% for the colored state. The change in optical density (Δ(OD)) (where Δ(OD) = −log ($T_{colored}/T_{bleached}$)) in the VIS region is thus 0.13. This value coincides with that calculated at 555 nm ($T_{bleached}$ = 41% and $T_{colored}$ = 58%). We recall that the human eye is sensitive to light waves for which the wavelength is between about 400 and 700 nm (visible region). Under abundant illumination (daylight) the maximum eye sensitivity lies in the green region at 555 nm (photopic vision) (dotted curve in Figure 9).

The switching speed (or device response time) of an ECD corresponds to the time required for the coloring/bleaching process. Among other factors, the switching speed depends on the ionic conductivity and thickness/morphology of the electrolyte and on the magnitude of the applied potential.[61] The response times of the prototype ECD reported here ($t \approx 50$ s) are fast.

The coloration efficiency (CE) of the glass/IZO/WO_3/d-PCL(530)/siloxane$_{6.1}$Li$_{12}$Eu$_{12}$/IZO/glass ECD was determined on the basis of CA measurements (Figure 10). The CE is a spectrally dependent parameter which measures the amount of charge necessary to produce the optical change. It is defined as the change in optical density per unit of inserted charge (CE = Δ(OD)/ΔQ). A high CE represents a large optical modulation at small charge insertion/desinsertion. During coloration from light yellow to uniform dark blue, a voltage of −4 V was applied during 50 s (Figure 10a) and charge, in the form of electrons and Li^+ ions, was transferred from the TCO and IC layers, respectively, to the EC layer (Scheme 2). Under these conditions, WO_3 suffered

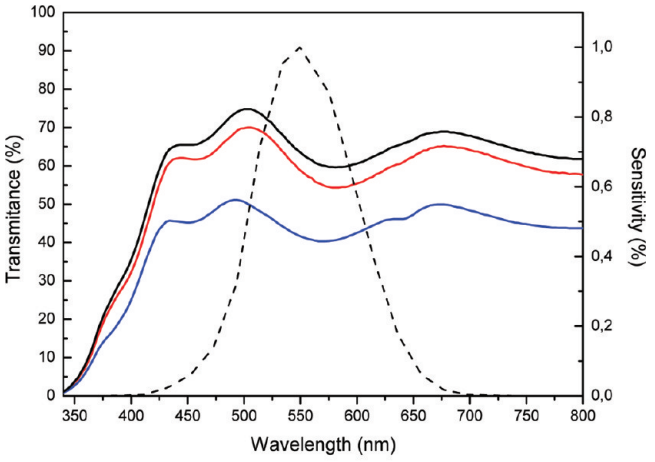

Figure 9. Transmission spectra of the as-deposited (black line), bleached (red line), and colored (blue line, 1st cycle) glass/IZO/WO_3/d-PCL-(530)/siloxane$_{6.1}$Li$_{12}$Eu$_{12}$/IZO/glass ECD. The pictures shown below the graphic reproduce the bleached and colored states of this ECD.

reduction and simultaneous Li^+ insertion. Upon reversing the polarity of the applied voltage, bleaching resulted (i.e., WO_3 was oxidated and Li^+ was desinserted) and the device recovered its initial state, i.e., from uniform dark deep blue to light yellow. In the present study, the device was cycled during a very short period of time (1500 s corresponding to 15 cycles) (Figure 10b). Figure 11 shows that the charge density decreases gradually with cycling, although this tendency is more abrupt during the first 5 cycles. It may be also inferred from Figure 11 that the ratio of the cathodic to the anodic charges (Q_{in}/Q_{out}) of the device decreases with cycling, demonstrating a progressive improvement of the charge insertion/desinsertion reversibility. For the second cycle a high CE value of 577 cm^2 C^{-1} was estimated for an Δ(OD) of 0.15. The short period of time covered by the CA measurements (only 15 cycles) does not enable us to comment of the stability of the glass/IZO/WO_3/d-PCL(530)/siloxane$_{6.1}$Li$_{12}$Eu$_{12}$/IZO/glass ECD.

The electrochromic memory of an ECD is the ability to hold its absorption state while the current is off. Figure 12 demonstrates that the open circuit memory of our prototype ECD is quite good (approximately 1 month).

The extremely encouraging results observed in this exploratory study confirm the advantages that derive from the use of the d-PCL(530)/siloxane$_{6.1}$Li$_{12}$Eu$_{12}$ material in ECDs. Further optimization of the procedures is obviously required, since improvements in switching speed, stability and optical memory and the application of lower operating voltages should be expected. Long-term operation of ECDs is known to depend critically on the production of defect-free ormolyte thin films and air-free

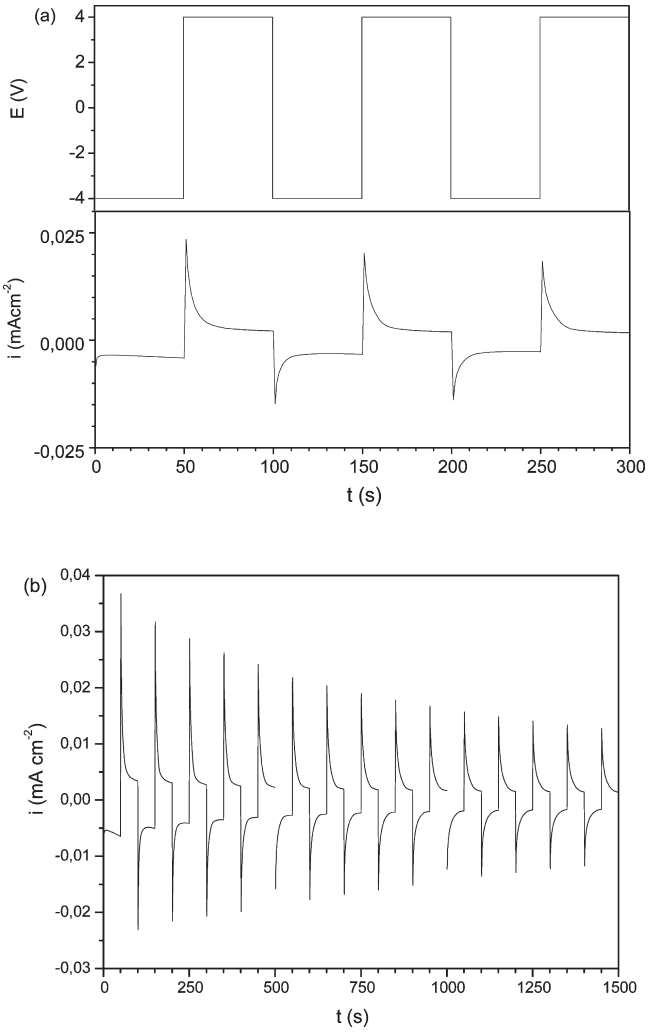

Figure 10. Time dependence of the current density of the glass/IZO/WO_3/d PCL(530)/siloxane$_{6.1}Li_{12}Eu_{12}$/IZO/glass ECD with potential steps of −4 and +4 V at every 50 s after (a) 3 and (b) 15 cycles. The area of the device was assumed to be ideally 4 cm^2.

sealing of the device.[61] The inclusion of a counter-electrode layer with high ion-storage capacity in future tests of this ECD is absolutely necessary to ensure the existence of a sufficient number of ions to produce a deep coloration of the WO_3 active EC layer and for the device to remain stable.

EXPERIMENTAL SECTION

α,ω-hydroxyl poly(ε-caprolactone) (PCL(530), Fluka, MW = 530 g mol^{-1}), 3-isocyanatepropyltriethoxysilane (ICPTES, Fluka, 95%), anhydrous $LiCF_3SO_3$ (Aldrich, 99.995%) and $Eu(CF_3SO_3)_3.xH_2O$ (Aldrich, 98%) were used as received. Ethanol (EtOH, Merck, PA grade) and tetrahydrofuran (Merck, puriss. PA grade) were stored over molecular sieves. High-purity distilled water was used in all experiments.

The synthetic method described elsewhere[43] was adopted to prepare the $LiCF_3SO_3$- and $Eu(CF_3SO_3)_3xH_2O$-doped d-PCL(530)/siloxane-based biohybrids. The molar ratio ICPTES: EtOH:H_2O used here was 1:4:1.5. Xerogels with different concentrations were produced as transparent and flexible monoliths. Relevant details of the synthetic procedure are presented in Table 1.

The thermal characteristics of the samples were determined by means of differential scanning calorimetry (DSC) and thermogravimetric

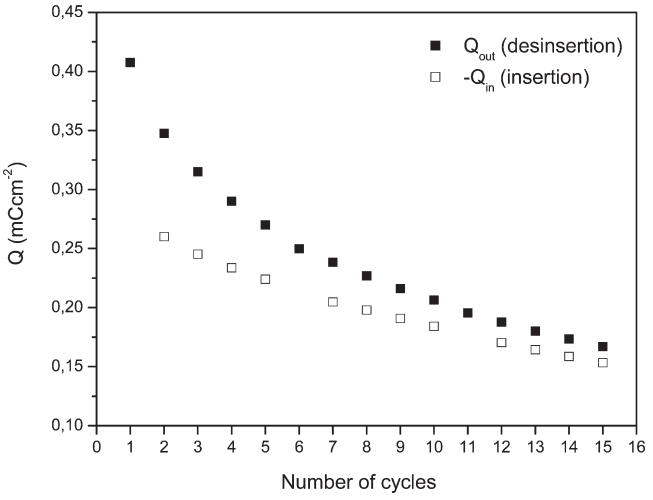

Figure 11. Charge density of the glass/IZO/WO_3/d PCL(530)/siloxane$_{6.1}Li_{12}Eu_{12}$/IZO/glass ECD as a function of the number of cycles: The area of the device was assumed to be ideally 4 cm^2. The data corresponding to the first insertion were discarded.

analysis (TGA). For the DSC experiments a disk section of the sample (hybrid film or powder) with a mass of approximately 10 mg was placed in a 30 μL aluminum can and stored in a desiccator over phosphorus pentoxide (P_2O_5) for one week at room temperature under vacuum. After this drying treatment the can was hermetically sealed and the thermogram was recorded using a DSC131 Setaram Differential Scanning Calorimeter. The sample was heated at 10 °C min^{-1} from 25 to 190 °C. For the TGA experiments the samples were first stored in a desiccator over P_2O_5. They were subsequently transferred to open platinum crucibles and analyzed from room temperature to 800 °C using a TA Instruments Q50 thermobalance at a heating rate of 10 °C min^{-1}. In both experiments the purge gas used was high purity nitrogen supplied at a constant 30 (DSC)/50 (TGA) cm^3 min^{-1} flow rate.

To evaluate the morphology of the samples, Scanning electronic microscopy (SEM) micrographs were obtained using a SEM/ESEM-FEI Quanta 400 scanning electron microscope at high acceleration voltage (20 kV). A small portion of the sample was cut, fixed on an aluminum stub with carbon tape and then coated with Au/Pd.

X-ray diffraction (XRD) patterns were recorded at room temperature using a Philips X'Pert MPD Powder X-ray diffractometer system. The films were exposed to monochromated CuK_α radiation (λ = 1.54 Å) over the 2θ range between 3 and 70° with a 2θ range resolution of 0.02. The samples, analyzed as films, were not submitted to any thermal pretreatment.

The total ionic conductivity of the ormolyte was determined by locating an electrolyte disk between two 10 mm diameter ion-blocking gold electrodes (Goodfellow, > 99.95%) to form a symmetrical cell. The electrode/ormolyte/electrode assembly was secured in a suitable constant-volume support[62] and installed in a Buchi TO51 tube oven. A type K thermocouple was placed close to the electrolyte disk to measure the sample temperature. Bulk conductivities of samples were obtained during heating cycles using the complex plane impedance technique at frequencies between 96 kHz and 500 mHz (Schlumberger Solartron 1250 frequency response analyzer and 1286 electrochemical interface), over a temperature range of 25 and 100 °C and at approximately 7 °C intervals.

Evaluation of the electrochemical stability window of electrolyte compositions was carried out within a dry argon-filled glovebox using a two-electrode cell configuration. Preparation of a 25 μm diameter gold microelectrode surface by the conventional polishing routine was

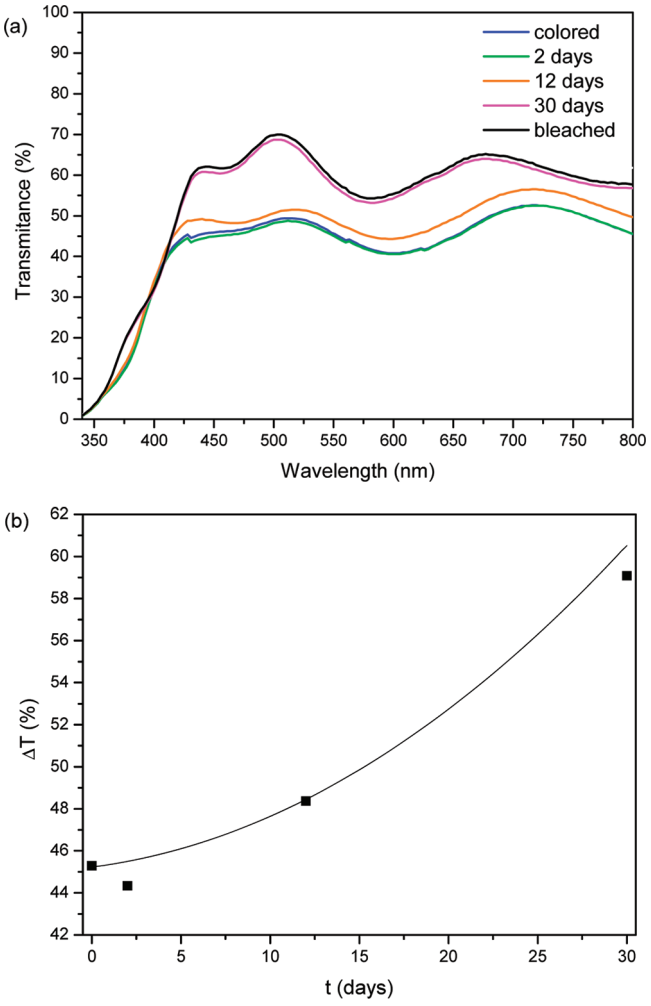

Figure 12. Time dependence of (a) the transmission spectra and (b) average transmittance in the VIS region of the glass/IZO/WO_3/d-PCL(530)/siloxane$_{6.1}$Li$_{12}$Eu$_{12}$/IZO/glass ECD. The transmittance of the colored state was measured after 15 cycles. The curve drawn in b is just a guide for the eyes.

completed outside the drybox prior to washing and drying before transfer into the drybox. The cell assembly was initiated by locating a clean lithium disk counter electrode (Aldrich, 99.9%, 10 mm diameter, 1 mm thick) on a stainless steel current collector. A thin-film sample of electrolyte was centered over the counter electrode and the cell assembly was completed by locating and supporting the microelectrode in the center of the electrolyte disk. The assembly was held together firmly with a clamp and electrical contacts were made to the Autolab PGSTAT-12 (Eco Chemie) used to record voltammograms at a scan rate of 100 mV s^{-1}. Measurements were conducted at room temperature within a Faraday cage located inside the measurement glovebox. The maximum potential range allowed by the equipment is 10 V.

The room-temperature photoluminescence spectrum of the complex was obtained using a ISS PC1 spectrofluorometer. The excitation device was equipped with a 300 W xenon lamp and a photographic grating. Emission spectra were collected with a 25 cm monochromator (resolution of 0.1 nm) connected to a photomultiplier. The excitation and emission slit width were fixed at 1.0 mm, with all used monochromators having 1200 grooves/mm. The experimental set up used for these lifetime measurements comprises a Nd:YAG (third harmonic)

Table 1. Details of the Synthesis of the d-PCL(530)/Siloxane$_n$Li$_m$Eu$_{m'}$ Hybrids

	n = 52.6		n = 27.0		n = 6.1		n = 3.2	
	Li^+	Eu^{3+}	Li^+	Eu^{3+}	Li^+	Eu^{3+}	Li^+	Eu^{3+}
	m = 99	m' = 111	m = 50	m' = 56	m = 12	m' = 12	m = 6	m' = 7
$1/n$ $1/m$	0.01	0.009	0.02	0.017	0.083	0.083	0.167	0.142
$1/n + 1/m$	0.019	52.6	0.037	27.0	0.163	6.1	0.309	3.2
$m_{PCL(530)}$ (g)	1.24		1.04		1.09		1.06	
v_{ICPTES} (μL)	1155		972		1024		988	
vH_2O (μL)	126		106		111		108	
v_{EtOH} (μL)	1006		929.78		979		945	
$m_{triflate\ salt}$ (g)	0.015	0.060	0.025	0.101	0.115	0.497	0.221	0.887

coherent laser of with λ = 355 nm used as excitation the source (frequency of 5 Hz and pulse width of 7 ns), a Tektronix TDS a 1012 oscilloscope and a fast detector ET 2000. The photoluminescence features of the hybrid material were recorded at room temperature with a modular double grating excitation spectrofluorimeter with a TRIAX 320 emission monochromator (Fluorolog-3, Horiba Scientific) coupled to a R928 Hamamatsu photomultiplier, using the front face acquisition mode. The excitation source was a 450 W Xe arc lamp. The emission spectra were corrected for detection and optical spectral response of the spectrofluorimeter and the excitation spectra were weighted for the spectral distribution of the lamp intensity using a photodiode reference detector. The lifetime measurements were acquired with the setup described for the luminescence spectra using a pulsed Xe−Hg lamp (6 μs pulse at half width and 20−30 μs tail).

The Fourier Transform infrared (FT-IR) spectra were acquired at room temperature using a Unicam FT-IR spectrophotometer. The spectra were collected in the 4000−500 cm^{-1} range by averaging 120 scans at a resolution of 4 cm^{-1}. About 2 mg of each sample were mixed with potassium bromide (Merck, spectroscopic grade) finely ground and pressed into pellets. The iterative least-squares curve-fitting procedure in the PeakFit (version 4)[63] software was used to decompose complex FT-IR band envelopes into the individual spectral components. Because of the disordered character of the materials under investigation, Gaussian band shapes were employed. A linear baseline correction with a tolerance of 0.2% was employed. The standard errors of the curve-fitting procedure were less than 0.03.

The indium-doped zinc oxide (IZO) was deposited on glass substrates by r.f. (13.56 MHz) magnetron sputtering using a ceramic oxide target of ZnO/In_2O_3 (5 cm diameter, Super Conductor Material, Inc., 99.99% purity). Sputtering was carried out at room temperature, under a partial pressure of oxygen of 2.5 × 10^{-3} Pa and a constant deposition pressure of 0.15 Pa. The distance between the substrate and the target was 10 cm and the r. f. power was held constant at 100 W.[64] The tungsten oxide (WO_3) film was prepared by thermal evaporation using WO_3 pellets (Super Conductor Materials, Inc., 99.99% purity). A deposition pressure of 1.6 × 10^{-3} Pa and a deposition rate of 10 nm/min were employed. The thickness of the IZO and WO_3 layers were 170 and 150 nm, respectively. Three prototype ECDs were tested. In the first stage of the assembly a small volume of the electrolyte sol (about 2 drops) was directly poured onto the surface of a 2 × 2 cm^2 WO_3/IZO-coated glass plate. A second IZO-coated glass plate was then placed on top of the hybrid electrolyte sol and the two plates were pressed together to spread the latter. In this manner a surface with an area of approximately 4 cm^2 was formed. The construction of the device was performed at room temperature. This assembly was kept for 24 h at these conditions to allow the drying procedure.

The optical transmittance of the ECD was measured in the 800−350 nm range with a UV−visible Spectronic Genexys 2PCC spectrophotometer.

Scheme 3. Close View of the Setup Used to Carry Out the CA Tests

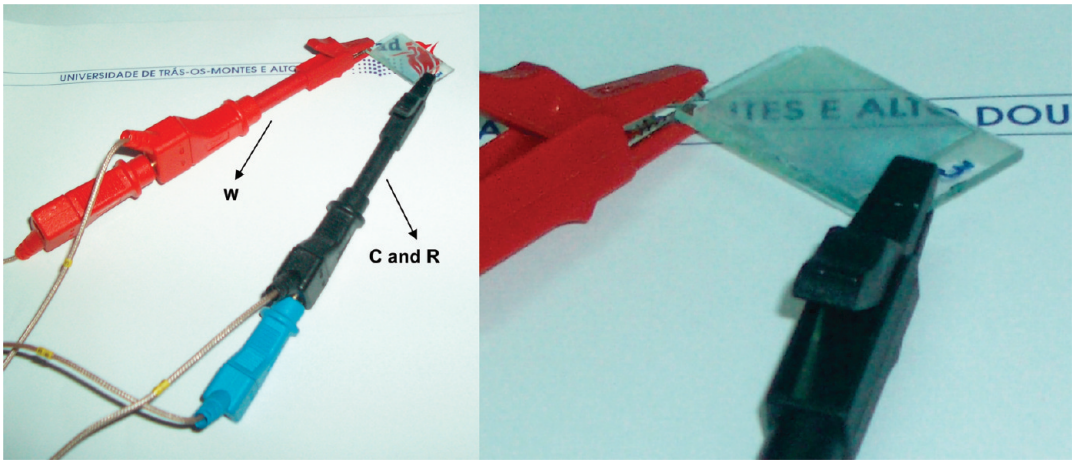

Chronoamperometric (CA) tests were performed using a potentiostat/galvanostat (Autolab model 100) by monitoring device current response as a function of time while the applied voltage was stepped between −4 V and +4 V with a delay time at each voltage of 50 s. The ECD was cycled 30 times between the colored and bleached states, respectively. In the setup used for measurements the electrolyte/WO_3/IZO substrate played the role of working electrode (W in Scheme 3) and the IZO substrate acted as counter and reference electrodes (C and R in Scheme 3). The cathodic and anodic charge densities were determined through integration of the CA curves during the coloring and bleaching processes, respectively.

CONCLUSIONS

The thermal (DSC and TGA), structural (XRD and FT-IR spectroscopy), electrochemical (ionic conductivity and CV) and photoluminescence properties of a novel series of $LiCF_3SO_3$- and $Eu(CF_3SO_3)_3$-doped diurethane cross-linked PCL(530)/siloxane biohybrids induced us to carry out preliminary tests of the performance of prototype ECDs incorporating these luminescent materials as electrolytes. The extremely promising results obtained for the switching time, optical density change, open circuit memory and high coloration efficiency lead us to foresee that these materials may find application in "smart windows" and other ECD-based devices, thus justifying further studies. However, several aspects will have to be taken into account in future for the improvement of their performance. The inclusion of counter-electrode layer with high ion-storage capacity is mandatory to ensure a sufficient number of ions for deeper coloration of the WO_3 layer at lower voltage, and therefore for the enhancement of both device stability and cyclability. The optimization of the ECD assembly procedure is another requirement that needs to be fulfilled. Problems related with the presence of air and/or defects in the electrolyte films produced during sealing might explain why the parameters deduced for the three prototype ECDs tested in this work, although not significantly different, did not match exactly. The control of moisture during device construction is also advisible. Another aspect that remains to examined is the variation of the $\Delta(OD)$ with ormolyte composition.

AUTHOR INFORMATION

Corresponding Author

*Phone: 00-351-259350253. Fax: 00-351-259350480. E-mail: vbermude@utad.pt.

Present Addresses

[§]CEA-LITEN/DTNM/LCSN, 17 rue des Martyrs, F 38054 Grenoble, Cedex 9, France

ACKNOWLEDGMENT

This work was supported by Fundação para a Ciência e a Tecnologia (FCT) and Projecto Estratégico - UI 686 - 2011-2012, PEst-C/QUI/UI0686/2011 and FEDER (PTDC/CTM/101324/2008). M.F., S.N., and L.C.R. acknowledge FCT for grants (SFRH/BD/38530/2007, SFRH/BD/28739/2006, and SFRH/BD/38616/2007, respectively).

REFERENCES

(1) Wright, P. V. *Br Polym J.* **1975**, *7*, 319–327.
(2) Armand, M.; Duclot, M. T.; Chabagno, J. M. In *Proceedings of the Second International Meeting on Solid State Electrolytes*; St. Andrews, Scotland, Sept 20−22, 1978; 1978; Extended Abstract 6.5
(3) Gray, F. M. In *Polymer Electrolytes*; RSC Materials Monographs; The Royal Society of Chemistry: London, 1997.
(4) Tarascon, J.-M.; Armand, M. *Nature* **2001**, *414*, 359–367.
(5) Carlos, L. D.; Videira, A. L. L. *Phys. Rev. B* **1994**, *49*, 11721–11728.
(6) Carlos, L. D.; Videira, A. L. L. *J. Chem. Phys.* **1994**, *101*, 8827–8830.
(7) Carlos, L. D.; Assunção, V; Alcácer, L. *J. Mater. Res.* **1995**, *10*, 202–210.
(8) Carlos, L. D.; Videira, A. L. L.; Assunção, M.; Alcácer, L. *Electrochim. Acta* **1995**, *40*, 2143–2146.
(9) Carlos, L. D.; Videira, A. L. L. *J. Chem. Phys.* **1996**, *105*, 8878–8885.
(10) Carlos, L. D.; Videira, A. L. L. *Chem. Phys. Lett.* **1997**, *264*, 57–62.
(11) Petersen, G.; Torell, L. M.; Panero, S.; Scrosati, B.; Silva, C. J. R.; Smith, M. J. *Solid State Ionics* **1993**, *60*, 55–60.
(12) Bernson, A.; Lindgren, J. *Solid State Ionics* **1993**, *60*, 31–36.
(13) Bernson, A.; Lindgren, J. *Solid State Ionics* **1993**, *60*, 37–41.
(14) Brodin, A.; Mattsson, B.; Torell, L. *J. Chem. Phys.* **1994**, *101*, 4621–4628.
(15) Silva, M. M.; Gonçalves, N.; Smith, M. J. *Electrochim. Acta* **1998**, *43*, 1511–1515.
(16) Silva, M. M.; Smith, M. J. *Electrochim. Acta* **2000**, *45*, 1463–1466.
(17) Lima, E., Mattos, R. I., Sentanin, F., Rodrigues, L. C., Silva, M. M. Ferreira, R. A. S., Carlos, L. D., Pawlicka, A. *Mater. Res. Innov.* **2011**, in press.

(18) Gadjourova, Z.; Andreev, Y. G.; Tunstall, D. P.; Bruce, P. G. *Nature* **2001**, *412*, 520–523.
(19) Berthier, C.; Gorecki, W.; Minier, M.; Armand, M. B.; Chabagno, J. M.; Rigaud, P. *Solid State Ionics* **1983**, *11*, 91–95.
(20) Berthier, C.; Gorecki, W.; Minier, M.; Armand, M. B.; Chabagno, J. M.; Rigaud, P. *Solid State Ionics* **1983**, *11*, 91–95.
(21) Carlos, L. D.; Ferreira, R. A. S.; de Zea Bermudez, V.; Julián-López, B.; Escribano, P. *Chem. Soc. Rev.* **2011**, *40*, 536–549.
(22) Gomez-Romero, P.; Sanchez, C. In *Functional Hybrid Materials*; Wiley Interscience: New York, 2003.
(23) Ravaine, D.; Seminel, A.; Charbouillot, Y.; Vincens, M. *J. Non-Cryst. Solids* **1986**, *82*, 210–219.
(24) Popall, M.; Andrei, M.; Kappel, J.; Kron, J.; Olma, K.; Olsowski, B. *Electrochim. Acta* **1998**, *43*, 1155–1161.
(25) Judeinstein, P.; Titman, J.; Stamm, M.; Schmidt, H. *Chem. Mater.* **1994**, *6*, 127–134.
(26) Dahmouche, K.; Atik, M.; Mello, N. C.; Bonagamba, T. J.; Panepucci, H.; Aegerter, M. A.; Judeinstein, P. *J. Sol−Gel Sci. Technol.* **1997**, *8*, 711–715.
(27) de Zea Bermudez, V.; Alcácer, L.; Acosta, J. L.; Morales, E. *Solid State Ionics* **1999**, *116*, 197–209.
(28) Wang, C.; Wei, Y.; Ferment, G. R.; Li, W.; Li, T. *Mater. Lett.* **1999**, *39*, 206–210.
(29) MacCallum, J. R.; Seth, S. *Eur. Polym. J.* **2000**, *36*, 2337–2341.
(30) Nishio, K.; Tsuchiya, T. *Sol. Energy Mater. Sol. Cells* **2001**, *68*, 295–306.
(31) Sanchez, C.; Julián, B.; Belleville, P.; Popall, M. *J Mater Chem.* **2005**, *15*, 3559–3592.
(32) de Zea Bermudez, V.; Silva, M. M. In *Polymer Electrolytes: Fundamentals and Applications*; Santos, D. M. F., Sequeira, C. A. C., Eds.; Woodhead Publishing Limited, Cambridge, MA, 2010; Chapter 7.
(33) Silva, M. M.; de Zea Bermudez, V.; Carlos, L. D.; Passos de Almeida, A. P.; Smith, M. J. *J. Mater. Chem.* **1999**, *9*, 1735–1740.
(34) Silva, M. M.; de Zea Bermudez, V.; Carlos, L. D.; Smith, M. J. *Electrochim. Acta* **2000**, *45*, 1467–1471.
(35) Sá Ferreira, R. A.; Carlos, L. D.; de Zea Bermudez, V. In *Encyclopedia of Nanoscience and Nanotechnology*; Nalwa, H. S., Eds.; American Scientific Publishers: Valencia, CA, 2004; Vol. 4, pp 719−762.
(36) Tunstall, D. P.; Tomlin, A. S.; Gray, F. M.; MacCallum, J. R.; Vincent, C. A. *J. Phys.: Condens. Matter.* **1989**, *1*, 4035–4045.
(37) Chowdari, B. V. R.; Huq, R.; Farrington, G. C. *Solid State Ionics* **1992**, *57* (1−2), 49–58.
(38) Latham, R. J.; Linford, R. G.; Pynenburg, R.; Schlindwein, W. S. *Electrochim. Acta* **1992**, *37*, 1529–1531.
(39) Giua, M.; Panero, V; Scrosati, B.; Cao, X.; Greenbaum, S. G. *Solid State Ionics* **1996**, *83* (1−2), 73–78.
(40) Morita, M.; Araki, F.; Yoshimoto, N.; Ishikawa, M.; Tsutsumi, H. *Solid State Ionics* **2000**, *136−137*, 1167–1173.
(41) Yang, H.; Farrington, G. C. *J. Polym.Sci., B: Polym. Phys* **2003**, *31* (2), 157–163.
(42) Chowdari, B. V. R.; Huq, R.; Farrington, G. C. *Electrochim. Acta* **1992**, *37*, 1667–1670.
(43) Nunes, S. C.; de Zea Bermudez, V.; Silva, M. M.; Smith, M. J.; Carlos, L. D.; Sá Ferreira, R. A.; Rocha, J. *J. Solid State Electrochem.* **2006**, *10*, 203–210.
(44) Teixeira, J. C. S.; Fernandes, M.; de Zea Bermudez, V.; Barbosa, P. C.; Rodrigues, L. C.; Silva, M. M.; Smith, M. J. *Electrochim. Acta* **2010**, *55*, 1328–1332.
(45) Fernandes, M.; de Zea Bermudez, V.; Sá Ferreira, R. A.; Carlos, L. D.; Charas, A.; Morgado, J.; Silva, M. M.; Smith, M. J. *Chem. Mater.* **2007**, *19*, 3892–3901.
(46) Lu, Zhenrong; Yang, L.; Guo, Y. *J. Power Sources* **2006**, *156*, 555–559.
(47) Chen, H. L.; Li, L.-J.; Lin, T.-L. *Macromolecules* **1998**, *31*, 2255–2264.
(48) Carlos, L. D.; de Zea Bermudez, V.; Sá Ferreira, R. A.; Marques, L.; Assunção, M. *Chem. Mater.* **1999**, *11*, 581–588.
(49) Skrovanek, D. J.; Howe, S. E.; Painter, P. C.; Coleman, M. M. *Macromolecules* **1985**, *18*, 1676–1683.
(50) Nunes, S. C.; de Zea Bermudez, V.; Ostrovskii, D.; Martins, N. V. *J. Mol. Struct.* **2008**, *879*, 72–80 and related references therein.
(51) Sanchis, A.; Prolongo, M. G.; Salom, C.; Masegosa, R. M. *J. Polym.Sci., Part B: Polym. Phys.* **1998**, *36*, 95–104.
(52) Wendsjo, A.; Lindgren, J; Thomas, J. O.; Farrington, G. C. *Solid State Ionics* **1992**, *53−56*, 1077–1082.
(53) de Zea Bermudez, V.; Ostrovskii, D.; Lavoryk, S.; Gonçalves, M. C.; Carlos, L. D. *Phys. Chem. Chem. Phys.* **2004**, *6* (3), 649–658.
(54) Huang, W.; Frech, R.; Wheeler, R. A. *J. Phys. Chem.* **1994**, *98*, 100–110.
(55) Stevens, J. R.; Jacobsson, P. *Can. J. Chem.* **1991**, *69*, 1980–1984.
(56) Jacobsson, P.; Albisson, I.; Mellander, B.-E.; Stevens, J. R. *Polymer* **1992**, *33*, 2778–2783.
(57) S. Ferreira, R. A.; Ferreira, A. L.; Carlos, L. D. *Eur. Phys. J. B* **2006**, *50*, 371–378.
(58) S. Ferreira, R. A.; Ferreira, A. L.; Carlos, L. D. *J. Non-Cryst. Solids* **2006**, *352*, 1225–1229.
(59) Livage, J.; D. Ganguli, D. *Sol. Energy Mater. Sol. Cells* **2001**, *68*, 365–381.
(60) Fortunato, E.; Pereira, L.; Barquinha, P.; Ferreira, I.; Prabakaran, R.; Goncalves, G.; Goncalves, A.; Martins, R. *Philos. Mag.* **2009**, *89*, 2741–2758.
(61) Argun, A. A.; Aubert, P.-H.; Thompson, B. C.; Schwendeman, I.; Gaupp, C. L.; Hwang, J.; Pinto, N. J.; Tanner, D. B.; MacDiarmid, A. G.; Reynolds, J. R. *Chem. Mater.* **2004**, *16*, 4401–4412.
(62) Silva, C. J. R.; Smith, M. J. *Electrochim. Acta* **1995**, *40*, 2389–2392.
(63) *PeakFit*; Jandel Corporation: San Rafael, CA
(64) Fortunato, E.; Pimentel, A.; Gonçalves, A.; Marques, A.; Martins, R. *Thin Solid Films* **2006**, *502*, 104–107.